Composites and Nano Engineering (2023)
Clausius Scientific Press, Canada

DOI: 10.23977/compne.2023.020102
ISSN 2616-1958 Vol. 2 Num. 1

Structure-magnetic and Morphology Properties of $La_{1-x}Sr_xMnO_3$ Nanomaterials by sol-gel

Jin Hao[1,2,#], Fengwu Du[2,#], Qing Lin[1,2,#], Pan Dong[2,*], Yun He[2], Fang Yang[1,*]

[1]College of Biomedical Information and Engineering, Hainan Medical University, Haikou, 571199, China
[2]College of Physics and Technology, Guangxi Normal University, Guilin, 541004, China
[#]These authors contributed equally to this work.
[*]Corresponding author

Keywords: Sol-gel, different preparation conditions, structure, magnetic properties

Abstract: In this paper, perovskite $La_{1-x}Sr_xMnO_3$ powder was successfully prepared by Sol-gel method. The effects of different doping amount, different pH value , different calcination temperature and different calcination time on the structure and magnetic properties of $La_{1-x}Sr_xMnO_3$ material were studied by XRD, SEM, FT-IR and VSM. When the doping amount is $x \geq 0.3$, the XRD shows that the sample is the perovskite material with cubic structure, and the doping amount is $x=0.3$, the SEM shows that the sample has a better particle morphology. The analysis of different pH values shows that the sample $La_{0.7}Sr_{0.3}MnO_3$ has the maximum specific saturation magnetization of 62.42 emu/g and the maximum coercivity of 66.87 Oe at pH=7. The analysis of different calcination temperatures shows that the sample $La_{0.7}Sr_{0.3}MnO_3$ has the maximum specific saturation magnetization of 62.42 emu/g and the maximum coercivity of 66.87 Oe, the calcination temperature is 1000℃. Different calcination time has little effect on the specific saturation magnetization and coercivity of the sample $La_{0.7}Sr_{0.3}MnO_3$, but it shows a decreasing trend. When the calcination time is 2h, it has the largest specific saturation magnetization and coercivity.

1. Introduction

In 1839 , researchers first discovered an inorganic material ($CaTiO_3$) in the metamorphic rocks of the Ural Mountains in Russia , and named it after the Russian mineralogist A. Von Perovski. Since then, the perovskite material with this structural feature has been and its structure began to enter the stage of scientific research [1-2]. The basic chemical formula of the perovskite material is ABO_3 , and its space group is P_{m3m} [3-5]. Perovskite nanomaterials (ABO_3)exhibit their unique advantages in various aspects due to their unique physical and chemical properties, among which $LaMnO_3$ oxides have a typical ABO_3 structure and an antiferromagnetic structure at room temperature [6-7].With $LaMnO_3$ as the parent body , with some divalent metals (Mg, Ca, Sr, Ba, etc.), monovalent metals (K, Na, etc.), transition metals, The mixed valence of +3 and +4 of Mn ions will appear, which leads to the emergence of ferromagnetic metallic states, accompanied by a huge magnetoresistance effect, which is a hot issue in the research of condensed matter physics in recent years [8-9].In recent years , there have been many studies on the structure and properties of $La_{1-x}Sr_xMnO_3$ materials[3], bcause

different preparation conditions have a great influence on the microstructure and magnetic properties of the synthesized samples. The effects of preparation conditions on the microstructure and magnetic properties of $La_{1-x}Sr_xMnO_3$ material samples are useful for further in-depth exploration of the intrinsic mechanism of $La_{1-x}Sr_xMnO_3$ -based oxide materials , as well as for novel functionalities. The application and development of materials and nanoelectronic devices are of great significance. In this paper, $La_{1-x}Sr_xMnO_3$ materials were prepared by Sol-gel method under different process conditions. The effects of different pH, impurity ratio of Sr element, calcination temperature and calcination time on $La_{1-x}Sr_xMnO_3$ were studied. The influence of the material's microstructure and magnetic properties is of great significance for further exploring the internal mechanism of A-site doped $LaMnO_3$ composite oxide materials , improving the application value of the material in the field of magnetism, and laying a foundation for the development of new materials.

2. Preparation and Characterization of Materials

2.1. Preparation of Materials

Experimeriment 3: (different calcination temperature)

Step 1: according to the molar ratio of $La_{0.7}Sr_{0.3}MnO_3$, weigh the total amount of $La(NO_3)_3$ and $Sr(NO_3)_2$, and 0.01 mol of $Mn(NO_3)_2$ (50%) solution , according to the mol ratio of the complexing agent and the metal ion to be 1:1 , take the citric acid monohydrate that the amount of the material is 0.02mol, and the weighed nitrate and the complex are respectively deionized water. Dissolving and mixing to obtain a precursor solution;

Step 2: the precursor solution is placed in a water bath at 50℃ and stirred , the pH of the solution is adjusted to 7 with ammonia water , and a small amount of ethylene glycol is added dropwise as a dispersant, and stirring and evaporation are continued until the solution is evaporated to dryness to obtain wet condensation glue.

Step 3: put the wet gel in a digital display drying box , dry it at 100℃ for 24 hours to obtain a dry gel , use alcohol self-propagating combustion to obtain a black precursor powder , fully grind the powder and put it in a muffle furnace , Then calcined at 400~1000℃ for 2 hours to obtain black and shiny sample powder.

Experiment 4: (different calcination time)

Step 1: according to the molar ratio of $La_{0.7}Sr_{0.3}MnO_3$, weigh the total amount of $La(NO_3)_3$ and $Sr(NO_3)_2$, and 0.01 mol of $Mn(NO_3)_2$ (50%)solution , according to the mol ratio of the complexing agent and the metal ion to be 1:1 , take the citric acid monohydrate that the amount of the material is 0.02mol, and the weighed nitrate and the complex are respectively deionized water. Dissolving and mixing to obtain a precursor solution;

Step 2: the precursor solution is placed in a water bath at 50℃ and stirred , the pH of the solution is adjusted to 7 with ammonia water , and a small amount of ethylene glycol is added dropwise as a dispersant, and stirring and evaporation are continued until the solution is evaporated to dryness to obtain wet condensation glue.

Step 3: put the wet gel in a digital display drying box , dry it at 100℃ for 24 hours to obtain a dry gel , use alcohol self-propagating combustion to obtain a black precursor powder , fully grind the powder and put it in a muffle furnace , The samples were calcined at 1000℃ for different time periods of 2 to 14 h to obtain black and shiny sample powders.

2.2. Characterization Method

In this paper, the X-ray diffractometer (D/max-2500v/pc) of Rigaku Company in Japan was used

to characterize and analyze the phase structure of the sample. The FT-IR spectrometer of PerkinElmer Company was used to analyze the possible functional groups and internal chemical bonds in the sample. The EVO18 electron scanning microscope of ZEISS company was used to test the microscopic morphology of the sample. The VSM-100 vibrating sample magnetometer of Yingpu Magnetics was used to test the hysteresis loop of the sample at room temperature.

3. Experimental Results and Discussion

3.1. XRD Analysis

The XRD pattern of $La_{1-x}Sr_xMnO_3$ (x=0 ~ 0.6) calcined at 1000℃ for 2 hours. It can be seen from the figure 1.The crystal structures of all samples conform to the perovskite structure. The ideal perovskite has a cubic structure with space group P_{m3m}, but the experimentally prepared samples with Sr doping ratio $x \leq 0.2$ have a certain degree of distortion in their crystal structures, which are rhombohedral (R-3C) structure, the lattice parameters of which are in perfect agreement with the standard card (JCPDS: 70-3942) values , which may be due to the higher activation energy provided under the experimental conditions with higher calcination temperature, which promotes the distortion of the crystal structure. When the doping ratio x>0.2 of Sr, the main peak changes from double peaks to single peaks, and the corresponding other peak positions also change from double peaks to single peaks. The diffraction peaks correspond to the perovskite materials with cubic structure , indicating that with the increase of the doping ratio of Sr, it is more conducive to the formation of the cubic phase structure. The reason for this change may be related to the lattice distortion caused by different Sr doping ratio.According to the calculation formula of tolerance factor $t=rA+ro/\sqrt{2}(r_B+r_o)$ and the ion mismatch degree formula $\sigma^2=\sum_i x_i r_i^2-\langle r_A \rangle^2$.The parameters of the t-factor and A-site ion mismatch σ^2 of the group samples are shown in Table 1. The calculation results show that with the increase of the doping ratio of Sr, t increases from 0.841 to 0.902 , indicating that with the doping of Sr As the ratio increases, the smaller the lattice distortion , the easier it is to form a stable perovskite structure.

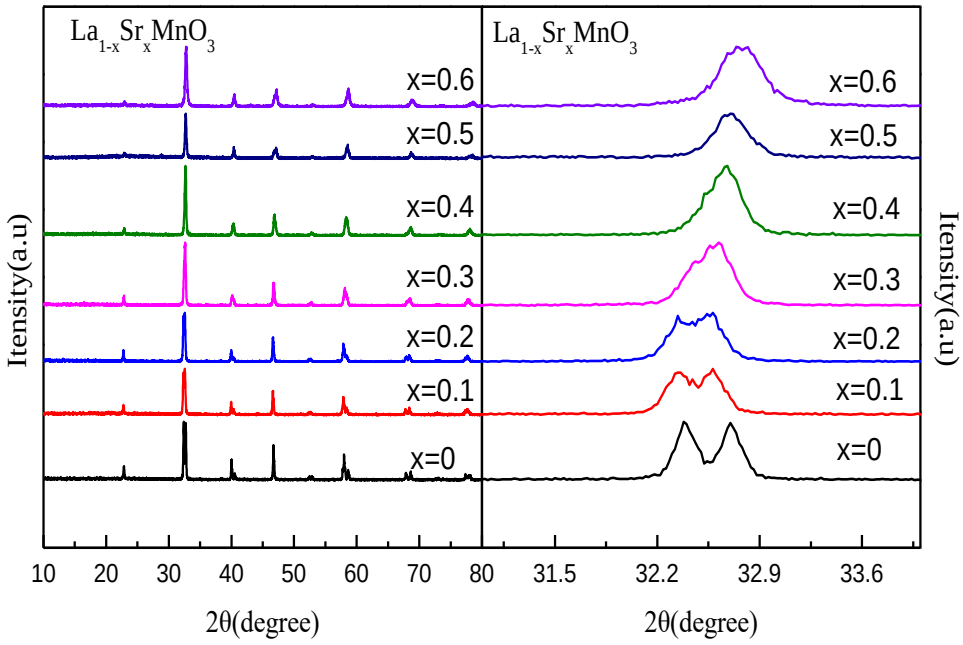

Figure 1: XRD of $La_{1-x}Sr_xMnO_3$ calcined at 1000℃ for 2 hours

Table 1: Parameters of $La_{1-x}Sr_xMnO_3$ calcined at 1000℃ for 2 h (sample tolerance factor t, mismatch σ^2 and grain size parameters)

parameter	x= 0	x= 0.1	x= 0.2	x= 0.3	x= 0.4	x= 0.5	x= 0.6
Space groups	R-3c(167)(hexagonal)	R-3c(167)(hexagonal)	R-3c(167)(hexagonal)	Pm-3m(221)(Cubic)	Pm-3m(221)(Cubic)	Pm-3m(221)(Cubic)	Pm-3m(221)(Cubic)
a(Å)	5.5218	5.5310	5.526 6	3.8856	3.8728	3.8706	3.8856
b(Å)	5.5218	5.5310	5.526 6	3.8856	3.8728	3.8706	3.8856
c(Å)	13.336	13.377	13.399	3.8856	3.8728	3.8706	3.8856
r_A	0.1032	0.104 7	0.106 2	0.1076	0.1091	0.1106	0.1121
r_B	0.0645	0.063 4	0.0622	0.061 1	0.0599	0.058 8	0.0576
r_O	0.14	0.14	0.14	0.14	0.14	0.14	0.14
t	0.841	0.851	0.860	0.871	0.881	0.892	0.902
σ^2	0	1.972	3.504	4.600	5.257	5.476	5.257
Vol($Å^3$)	352.14	354.4	354.43	58.67	58.08	57.99	58.66
Density(g/cm^3)	6.8426	6.7989	6.7983	6.8453	6.9139	6.9256	6.8457
Crystallite Size(A)	35.7019	23.9441	24.623 9	29.1053	31.438 7	35.7270	29.6014

Taking $LaMnO_3$ as an example, as shown in Figure 2 , La^{3+} with larger ionic radius is located at the top corner of the simple cube , Mn^{3+} with smaller ionic radius is located in the center of the cube , and O^{2-} is located at the corner of the cube. Face-centered , the main feature of this structure is that Mn-O ions form MnO_6 octahedral structure , which is connected with La^{3+} at the top corners to form a spatial network. Table 1 also gives the lattice parameter table of samples $La_{1-x}Sr_xMnO_3$ (x=0 ~ 0.6) calcined at 1000℃ for 2 hours.

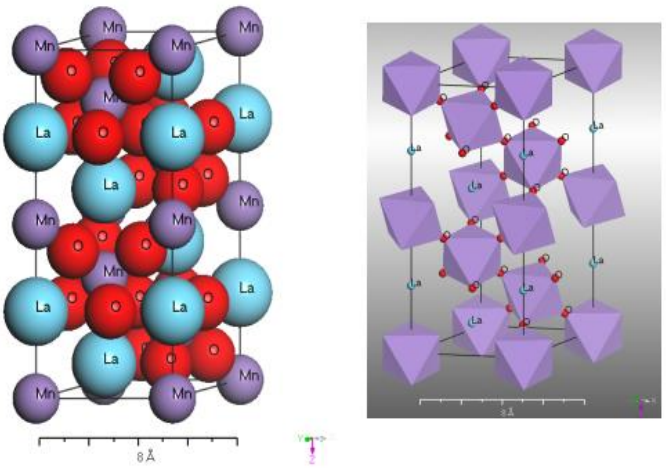

Figure 2: Structure diagram of $LaMnO_3$

It can be seen from the peak shift diagram in Figure 1, with the increase of doping ratio , when $x \leq 0.2$, the main peak shifts to low angle first , and its lattice parameters also change correspondingly, according to the Bragg equation $2d\sin\theta = n\lambda$ is known , λ is constant , the smaller the θ, the larger the d, and the larger the unit cell parameter , corresponding to the increasing trend of the volume in Table 1 , indicating that after the doped Sr atoms replace the La atoms into the $LaMnO_3$ lattice. The lattice distortion causes the size of the unit cell to become larger; and x>0.2 , the position of the peak shifts to a high angle with the increase of the doping ratio of Sr. According to the Bragg equation $2d\sin\theta = n\lambda$,

λ is constant , and the larger the θ, the higher the angle. The smaller the d, the smaller the unit cell parameters, corresponding to the decreasing trend of the volume in Table 1. The reason for the decrease may be that the substitution of Sr will cause the change of the size of the A site and the change of the valence state of Mn , although the Sr^{2+} ionic radius (0.118nm) is close to La^{3+} ionic radius (0.1032nm) , with the increase of Sr substitution amount *x*, in order to maintain the electrical neutrality of the whole compound[2] , B-site Mn^{3+} (ionic radius 0.0645nm) is oxidized Mn^{4+} (ionic radius 0.0530nm) is formed, and the content of Mn^{4+} increases, the covalency between Mn and O ions increases, and the atomic orbitals between Mn -O overlap more, resulting in a decrease in the unit cell volume[4]. Another factor that affects the unit cell volume is the oxygen content in the compound. With the increase of the Mn substitution amount *x*, the perovskite structure will generate oxygen vacancies, which may also lead to changes in the unit cell volume.In addition , the average grain size D of the sample can be calculated from the full width at half maximum (FWHM) of the main diffraction peak using the Scherrer formula: $D=0.94\lambda/\beta \cos\theta$, where λ is the x-ray wavelength and θ is the diffraction angle, the average grain sizes of the crystals were calculated to be 35.7019nm, 23.9441nm, 24.6239nm, 29.1053nm, 31.4387nm, 35.7270nm, 25.1403nm, the samples were nanoparticles.

Figure 3 is the XRD diffraction pattern of the sample $La_{0.7}Sr_{0.3}MnO_3$ calcined at 400℃, 500℃, 600℃, 700℃, 800℃, 900℃, and 1000℃ for 2 h. When the calcination temperature is 400℃, the sample begins to generate corresponding diffraction peaks and impurity phases are generated. As the calcination temperature increases, the diffraction peaks tend to be complete and the impurity phases decrease. When the temperature rises to 700℃, no impurity phase disappears, and the diffraction peaks are very sharp, forming a unique perovskite structure. After comparing with the standard card (ICSD NO. 75-0440), these diffraction peaks correspond to the perovskite with cubic structure respectively. With the continuous increase of calcination temperature, the main diffraction peak is further enhanced. By Scherrer's formula: $D=0.94\lambda/\beta\cos\theta$, the average grain size D of the sample can be calculated from the full width at half maximum (FWHM)of the main diffraction peak, where λ is the x-ray wavelength and θ is the diffraction angle. As shown in Table 2, The average grain sizes of the obtained crystals were 17.5234 nm, 18.8254 nm, 18.2343 nm, 20.4325 nm, 23.2957 nm, 25.5735 nm, 29.6014 nm, the samples were nanoparticles, and with the increase of calcination temperature, the average grain size shows an increasing trend, indicating that the crystallinity of the sample is more complete.

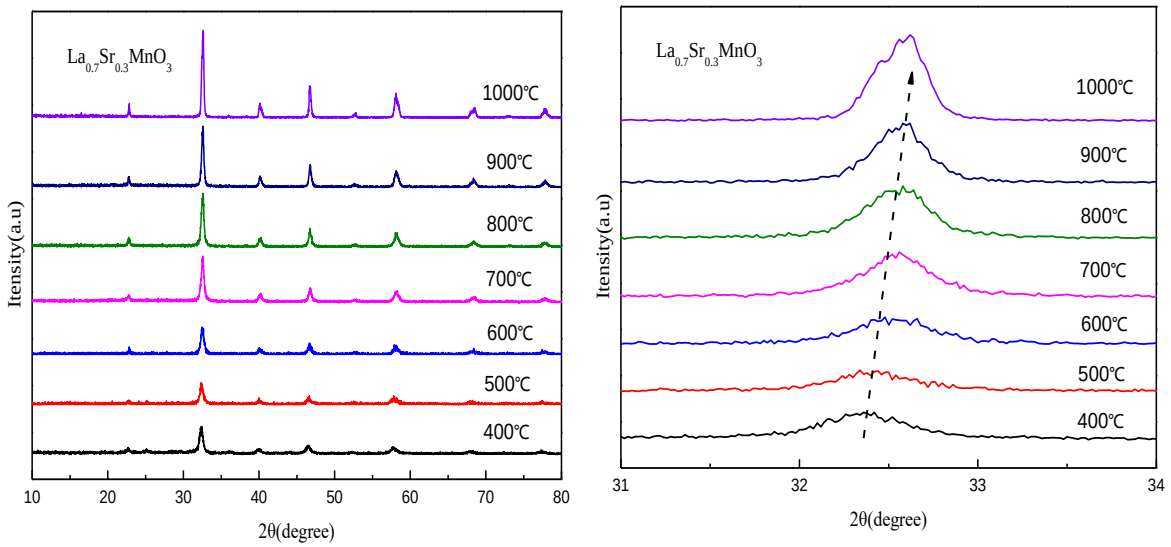

Figure 3: XRD of $La_{0.7}Sr_{0.3}MnO_3$ calcined at different temperatures for 2 hours

Table 2: XRD parameters of $La_{0.7}Sr_{0.3}MnO_3$ calcined at different temperatures for 2 hours

Parameter	400	500	600	700	800	900	1000
Space groups	Pm-3m (221) (Cubic)	Pm-3m (221) (Cubic)	Pm-3m (221) (Cubic)	Pm-3m (221) (Cubic)	Pm-3m (221) (Cubic)	Pm-3m (221) (Cubic)	Pm-3m (221) (Cubic)
a(Å)	3.89559	3.88946	3.87943	3.88375	3.88164	3.87923	3.88555
Vol(Å ^{3})	59.12	58.84	58.39	58.58	58.49	58.38	58.66
Density(g/cm3)	6.7930	6.8251	6.8782	6.8552	6.8665	6.8793	6.8457
Fit Size XS(nm)	17.523 4	18.825 4	18.2343	20.4325	23.295 7	25.5735	29.601 4
Fhwn	0.493	0.459	0.474	0.423	0.371	0.338	0297

3.2. SEM Analysis

Figure 4 shows the SEM images of (1) $La_{0.9}Sr_{0.1}MnO_3$ (2) $La_{0.7}Sr_{0.3}MnO_3$ (3) $La_{0.5}Sr_{0.5}MnO_3$ samples. The different ratios of Sr doping were used to prepare the $La_{1-x}Sr_xMnO_3$ samples have different characteristics, when the doping ratio x=0.1, the sample has more serious particle agglomeration and blurred grain boundaries, and as the doping ratio increases, the agglomeration between particles decreases, when the doping ratio x=0.5, the agglomeration between the particles is the least, and the boundary is clear, but the particle size of the samples is inconsistent, which may be related to the preparation process conditions and the eg electrons of the Mn atoms make the octahedron formed by oxygen. It is related to the occurrence of Jahn-Teller distortion. When the doping ratio is small, the tolerance factor is small, and it is easy to distort the lattice, resulting in strong interaction between grains, resulting in agglomeration. In addition, with the doping ratio of Sr As the Sr ion radius is larger than the La ion radius, the A-site ion mismatch degree of the sample doped with a high proportion further increases, causing the mismatch between adjacent layers, which is easy to distort the lattice, resulting in The structure changes, the macroscopic particle shape becomes irregular, and the particle size is inconsistent.According to the statistics of the particle distribution analysis software, the particle size of the sample is mainly concentrated in the range of 28-68.8nm, and the Scherrer formula to calculate the average grain size to be 24.9065nm, indicating that the sample prepared in the experiment is the polycrystalline material.

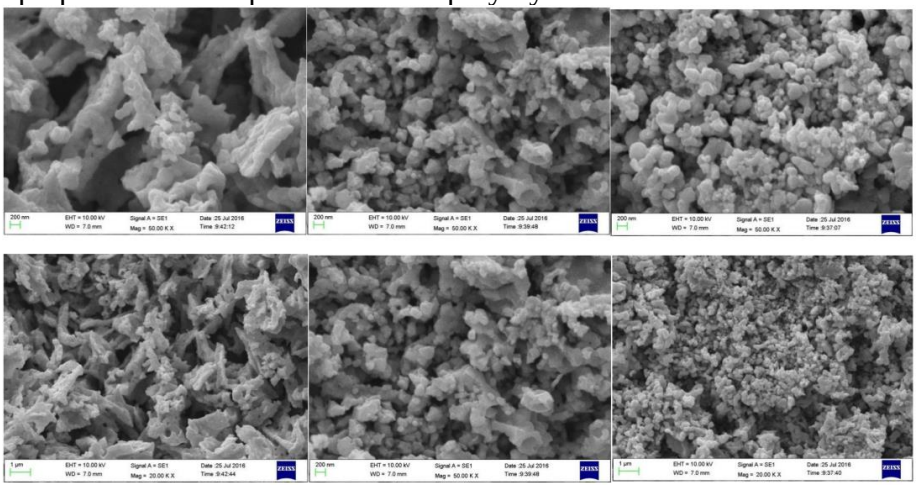

(1) $La_{0.9}$ $Sr_{0.1}MnO_3$, (2) $La_{0.7}Sr_{0.3}MnO_3$, (3) $La_{0.5}$ $Sr_{0.5}MnO_3$

Figure 4: SEM images of $La_{1-x}Sr_xMnO_3$ calcined at 1000℃ for 2 hours

3.3. Infrared Analysis

Figure 5 presents the FT-IR images of $La_{1-x}Sr_xMnO_3$, with KBr as the background, the diagrams indicate the absorption at the low-frequency wavenumber stage in the main band around 450-600 cm^{-1} peaks, which can be attributed to the Mn-O stretching vibration and the O-Mn-O bending vibration in the MnO_6 regular octahedron caused by the Jahn-teller distortion, including the changes of its bond length and bond angle, which are related to its vibrational state [1,10]. There is a narrow vibrational peak at the wavenumber of about 1384 cm^{-1}, which is the asymmetric stretching vibration of the metal carbonate[1,11], a small vibrational peak at the wavenumber of about 1056 cm^{-1} reflects the stretching vibration of the carboxyl radical [2,5], a very small peak near 2900 cm^{-1} may be due to the impurity $SrCO_3$, or the combined effect of CH_3 , CH_2 and OH[6, 8]. There is a broad peak at about 3436 cm^{-1} corresponding to the stretching vibration of water molecule OH [9, 10], and a strong absorption peak at 1630 cm^{-1} is attributed to the bending vibration of surface water molecule HOH [11, 12]. In addition , it can be seen from the XRD pattern that the sample has produced corresponding perovskite diffraction peaks at 400°C. Combined with the FT-IR pattern, it can be found that the CH and CC framework vibration peaks in the sample due to organic matter have disappeared [13].All in all, the stretching vibration peaks appearing from the spectra indicate that all the as-prepared samples form perovskite structures, which are consistent with our conclusions obtained from XRD diffraction.

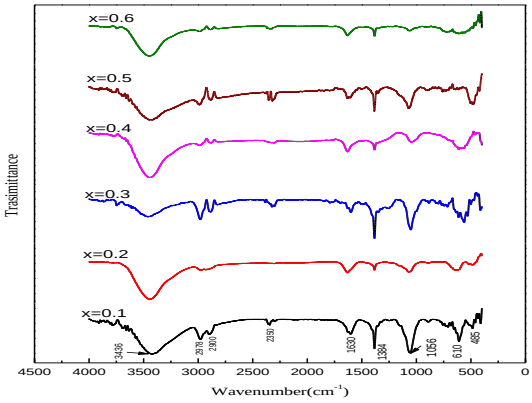

Figure 5: FT-IR images of $La_{1-x}Sr_xMnO_3$

3.4. Magnetic Analysis

The experimental phenomena of the preparation of $La_{0.7}Sr_{0.3}MnO_3$ materials at different PH. It can be seen from Table 3, with PH=1 , the precursor solution is a colorless solution, and with PH=3 and PH=5, both a stable gel cannot be formed , and finally a white blocky dry gel is obtained; with PH=7 or PH=9 , the sol is a yellow clear solution , and a reddish-brown gel is obtained.

Table 3: The experimental phenomena in the process of preparing $La_{0.7}Sr_{0.3}MnO_3$ materials at different PH

PH value	Sol	gel	dry glue	sample powder
PH=1	colorless	yellow	brown	black
PH=3	white precipitate	White	White	black
PH=5	pale yellow solution	Brick red	White	black
PH=7	yellow clear liquid	Red-brown	Red-brown	black
PH=9	yellow clear liquid	Red-brown	Red-brown	black

Table 4 shows magnetic parameters of $La_{0.7}Sr_{0.3}MnO_3$ calcined at 1000°C for 2 hours at different pH. It can be seen from Table 4 that with the increase of pH value, the specific saturation

magnetization of the sample first increases and then decreases. When PH=7, the sample has the maximum specific saturation magnetization of 62.42 emu/g. In addition , it can be seen from Table 4 that with the increase of pH value, the coercive force also increases first and then decreases. When PH=7, the sample has the maximum coercive force of 66.87 Oe.

Table 4: Magnetic parameters of $La_{0.7}Sr_{0.3}MnO_3$ calcined at 1000℃ for 2 h at different pH

Parameter	PH=1	PH=3	PH=5	PH=7	PH=9
M_S (emu/g)	26.30	49.40	55.82	62.42	55.77
H_C (Oe)	41.28	51.06	55.89	66.87	56.03

Figure 6 shows the hysteresis loop of $La_{1-x}Sr_xMnO_3$ at room temperature. The pure $LaMnO_3$ powder has antiferromagnetic properties. The hysteresis loops are all closed curves, showing obvious ferromagnetism at room temperature, and the magnetization basically reaches saturation around 0.2T , which is a soft magnetic material with small coercivity. Table 5 shows $La_{1-x}Sr_xMnO_3$ calcined at 1000℃ for 2 hours, the specific saturation magnetization of the samples are 32.03 emu/g, 56.78 emu/g, 62.42 emu/g, 51.38 emu/g, 23.52 emu/g, 12.50 emu/g. With the increase of doping ratio, the specific saturation magnetization first increases and then decreases, when the doping ratio x=0.3, the $La_{1-x}Sr_xMnO_3$ has the largest specific saturation magnetization, which has the value of 62.42 emu/g.

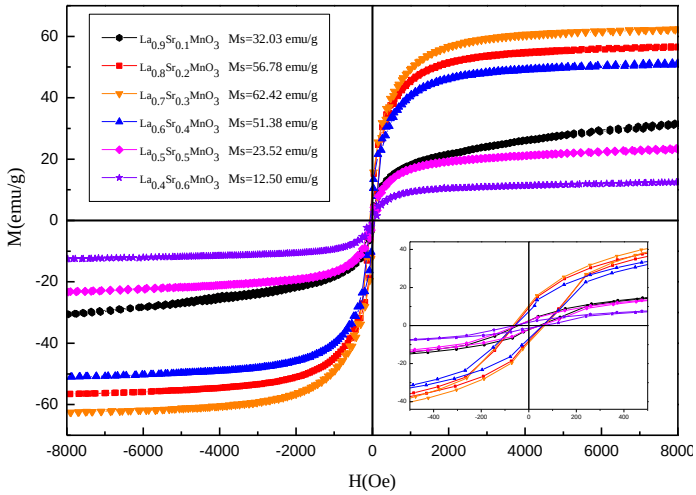

Figure 6: Magnetic properties of $La_{1-x}Sr_xMnO_3$ calcined at 1000℃ for 2 h

Table 5: Magnetic parameters of $La_{1-x}Sr_xMnO_3$ calcined at 1000℃ for 2 h

x	0.1	0.2	0.3	0.4	0.5	0.6
M_S (emu/g)	32.03	56.78	62.42	51.38	23.52	12.50
M_r (emu/g)	2.46	9.44	10.44	7.33	2.47	1.62
M_r / M_S	0.077	0.166	0.167	0.143	0.105	0.130
H_C (Oe)	43.93	60.13	66.87	58.20	50.25	59.96

When the A site of $LaMnO_3$ is replaced by a part of cations, in order to maintain the balance of the whole valence, the manganese ions in it generate mixed valence states of Mn^{3+} and Mn^{4+}. When the bond angle of the Mn-O-Mn coupling is 180 °, its energy distribution is shown in Figure7, the electronic configuration of Mn^{4+} is $3d^3(t_{2g}^3e_g)$, since the e_g orbital is closely related to the the energy of the 2p orbital of O^{2-} , and it is easy to transfer an electron on the 2p orbit of O^{2-} to the empty orbit of Mn^{4+}, as shown in Figure 7.

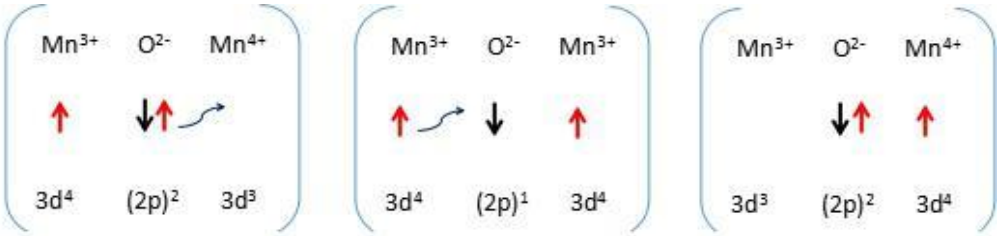

Figure 7: Schematic diagram of double exchange between manganese ions

While the adjacent Mn^{3+} the electrons on the eg orbital of the ion are filled to the 2p orbital of O^{2-}, which is the double exchange effect, and the traveling electron e_g is freely exchanged between Mn^{3+} and Mn^{4+} to form the conductance. At the same time, it is constrained by Hund's law to keep parallel alignment with the t_{2g} electrons, which leads to the appearance of ferromagnetism. During the entire exchange process, the energy of the system remains unchanged. When an external magnetic field is applied, the resistivity decreases due to the orientational ordering of the localized spins, resulting in a negative CMR effect. According to the double exchange model, when the ratio of the number of Mn^{4+} to Mn^{3+} ions is 1:2, eg electrons can be continuously transferred between adjacent Mn^{4+} and Mn^{3+} ions, and the double exchange effect is the strongest at this time. On the other hand, the ratio of Mn^{4+}/Mn^{3+} of 1:2 is also favorable for the formation of an ideal cubic perovskite structure, and any deviation from the ideal cubic perovskite structure will lead to lattice distortion and reduce Mn-O-Mn bond angle, weakening the double exchange. Therefore, in the $La_{1-x}Sr_xMnO_3$ system, the ratio of the number of Mn^{4+} to Mn^{3+} ions of $La_{0.7}Sr_{0.3}MnO_3$ is close to 1:2 , and has a higher specific saturation magnetization.

Figure 8 shows the magnetic images of $La_{0.7}Sr_{0.3}MnO_3$ calcined at different temperatures for 2 hours. The sample exhibits obvious ferromagnetism with the increase of temperature. When the temperature is 1000℃, the The specific saturation magnetization is the largest; and the calcination temperature exceeds 1000℃ , the specific saturation magnetization of the sample begins to decrease again, which may be because the crystal structure tends to be complete with the increase of the calcination temperature. However, when the temperature increases to 1000℃, the specific saturation magnetization tends to be saturated. Continuing to increase the calcination temperature will easily cause the crystals to agglomerate, thereby reducing the specific saturation magnetization. Table 6 gives the magnetic parameters of $La_{0.7}Sr_{0.3}MnO_3$ calcined at different temperatures for 2 hours, it can be seen from the Table 6 that with the increase of the calcination temperature of the sample, the specific saturation magnetization first increases and then decreases. The sample has the largest specific saturation magnetization of 64.24 emu/g.

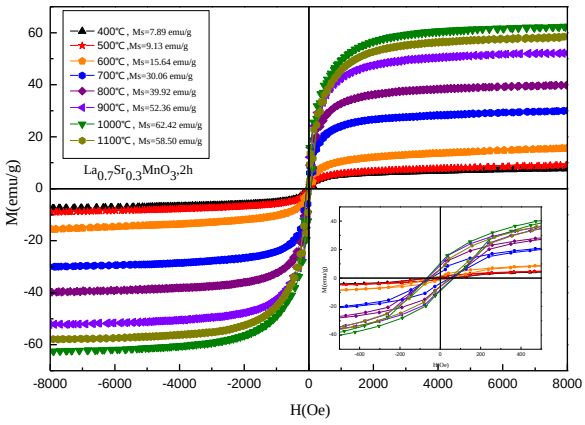

Figure 8: Magnetic properties of $La_{0.7}Sr_{0.3}MnO_3$ calcined at different temperatures for 2 h

Table 6: Magnetic parameters of $La_{0.7}Sr_{0.3}MnO_3$ calcined at different temperatures for 2 hours

Calcination temperature (℃)	400	500	600	700	800	900	1000	1100
M_S (emu/g)	7.87	9.13	15.64	30.06	39.92	52.36	62.42	58.50
M_r (emu/g)	0.83	0.85	1.44	3.96	6.31	8.92	10.44	6.13
M_r / M_S	0.106	0.097	0.092	0.132	0.158	0.170	0.167	0.105
H_C (Oe)	53.54	48.65	41.46	46.73	55.87	65.26	66.87	46.27

Figure 9 shows the magnetic images of $La_{0.7}Sr_{0.3}MnO_3$ calcined at 1000℃ for different times. Al the samples show ferromagnetism. Table 7 shows that $La_{0.7}Sr_{0.3}MnO_3$ calcined at 1000℃ for different times. It can be seen from the Table 7 that different calcination time has little effect on the specific saturation magnetization, remanent magnetization and coercivity of the samples, but the magnetic parameters show the decreasing trend.

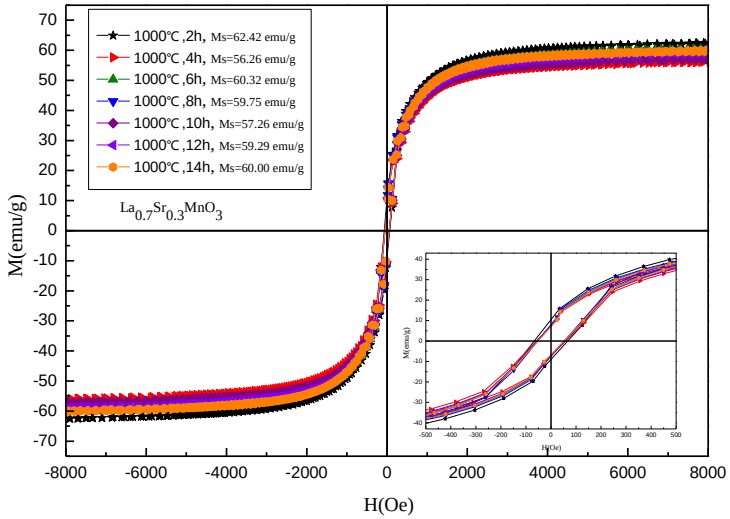

Figure 9: Magnetic properties of $La_{0.7}Sr_{0.3}MnO_3$ calcined at 1000℃ for different times

Table 7: Magnetic parameters of $La_{0.7}Sr_{0.3}MnO_3$ calcined at 1000℃ for different time

Calcination time (H)	2	4	6	8	10	12	14
M_S (emu/g)	62.42	56.26	60.32	59.75	57.26	59.29	60.00
M_r (emu/g)	10.44	7.34	7.64	7.97	7.60	7.45	7.05
H_C (Oe)	66.87	57.76	55.62	53.04	55.55	54.28	51.84

4. Conclusion

Through the research in this paper, it is found that different doping amounts have a great influence on the grain structure and magnetic properties of the samples. XRD shows that with the increase of the doping ratio of Sr, the smaller the lattice distortion, the easier it is to form stable calcium titanite structure, when the doping amount $x \geq 0.3$, the sample is a perovskite material with a cubic structure. SEM shows that the samples with different doping amounts have different morphological characteristics. When the doping amount $x=0.3$, the SEM shows that the morphology of the sample is better. The VSM shows that with the increase of doping amount, the saturation magnetization and coercivity first increase and then decrease. When the doping amount is $x=0.3$, the sample has saturation magnetization and coercivity. Therefore, the optimal doping amount is 0.3. The influence of different pH values on the magnetic properties of the samples. When the pH value is 7, the sample

$La_{0.7}Sr_{0.3}MnO_3$ has the maximum specific saturation magnetization of 62.42 emu/g and the maximum coercivity of 66.87 Oe. Therefore, the optimal pH is 7. The influence of different calcination temperatures on the magnetic properties of the samples, VSM shows that with the increase of calcination temperature, the saturation magnetization and coercivity first increase and then decrease. The specific saturation magnetization is 62.42 emu/g, and the maximum coercivity is 66.87 Oe. Therefore, the optimal calcination temperature is 1000℃. The influence of different calcination time on the magnetic properties of the sample, VSM shows that with the increase of calcination time, the saturation magnetization and coercivity have little change but show a decreasing trend. When the calcination time is 2h, the sample $La_{0.7}Sr_{0.3}MnO_3$ has the largest specific saturation magnetization of 62.42 emu/g, and has the largest coercivity of 66.87 Oe. Therefore, the optimal calcination time is 2h. The optimal experimental conditions determined in this paper can provide experimental reference and reference for other researches.

Acknowledgment

This work was financially supported by the National Natural Science Foundation of China (NO.11364004). J. Hao and F.Du contributed equally to this work. All authors discussed the results and commented on the manuscript.F. Yang and P. Dang are co-corresponding authors contributed equally.

References

[1] Ahmad Gholizadeh, Azim Malekzadeh, Mahnaz Ghiasi. Preparation, Structural and magnetic features of $La_{0.7}Sr_{0.3}Mn_{1-x}CO_xO_3$ nano-catalysts for ethane combustion and co oxidation. Ceramics International, 2016, 133: 1-11.

[2] J. I. A. Abdel-Latif, AdelA. Ismail, HoucineBOuzid, A. Al-Hajry Synthesis of novel perovskite crystal structure phase of strontium doped rare earth manganites using sol gel method. Journal of Magnetism and Magnetic Materials, 2015, 393: 233-238.

[3] Saitoh E, Okamoto S, Takahashi K T, et al. Observation of orbital waves as elementary excitations in a solid. Nature, 2001, 410(6825):180-183.

[4] Sharma J N, Sharma K K, Kumar A. Surface waves in a piez Oelectric–semiconductor composite structure - ScienceDirect. International Journal of Solids & Structures, 2010, 47(6):816-826.

[5] Pecchi G, Campos C, Pea O, et al. Structural, magnetic and catalytic properties of perovskite-type mixed oxides $LaMn_{1-y}Co_yO_3$ (y=0. 0, 0. 1, 0. 3, 0. 5, 0. 7, 0. 9, 1. 0). Journal of Molecular Catalysis A Chemical, 2008, 282(1):158-166.

[6] P. Kulandaivelu, K. Sakthipandi, P. SenthilKumar, V. Rajendran Mechanical properties of bulk and nanostructured $La_{0.61}Sr_{0.39}MnO_3$ perovskite manganite materials. Journal of Physics and Chemistry of Solids, 2013, 74: 205-214.

[7] Keshri S, Joshi L, Rout S K. Influence of BTO phase on structural, magnetic and electrical properties of LCMO. Journal of Alloys & Compounds, 2009, 485(1-2):501-506.

[8] Kolat V S, Gencer H, Gunes M, et al. Effect of B-doping on the structural, magnetotransport and magnetocaloric properties of $La_{0.67}Ca_{0.33}MnO_3$ compounds. Materials Science & Engineering B, 2007, 140(3):212-217.

[9] ARPSC, BBMN, BGTC, et al. Solution combustion derived nanocrystalline macroporous wollastonite ceramics. Materials Chemistry and Physics, 2006, 95(1):169-175.

[10] Sakthipandi K, Rajendran V. On-line phase transitions of bulk and nanocrystalline $La_{1-x}Pb_xMnO_3$ (x=0. 3, 0. 4, 0. 5) perovskite manganite materials using ultrasonic measurements. Materials Chemistry and Physics, 2013, 138(2): 581-592.

[11] K Sakthipandi, and, et al. Synthesis and on-line ultrasonic characterisation of bulk and nanocrystalline $La_{0.68}Sr_{0.32}MnO_3$ perovskite manganite. Journal of Alloys and Compounds, 2011, 509(8):3457-3467.

[12] Gehrke K, Moshnyaga V, Samwer K, et al. Interface controlled electronic variations in correlated heterostructures. Physical Review B, 2009, 82(11):113101.

[13] Venkataiah G, Krishna D C, Vithal M, et al. Effect of sintering temperature on electrical transport properties of $La_{0.67}Ca_{0.33}MnO_3$. Physica B Condensed Matter, 2005, 357(3-4):370-379.